Physical Review E **83** (2011) 021604 (*14 pages*)

The effect of ultrafast diffusion on adsorption, desorption and reaction processes over heterogeneous surfaces

A. García Cantú Ros*, J.-S. McEwen†, and P. Gaspard
Center for Nonlinear Phenomena and Complex Systems, Campus Plaine, Code Postal 231, Université Libre de Bruxelles, B-1050 Brussels, Belgium

The effect of ultrafast diffusion is studied on reaction-diffusion processes in heterogeneous media, as encountered in catalysis and field emission microscopy. The reaction-diffusion equations describe adsorption, desorption, and reaction processes for two adspecies, for instance, on a paraboloidal heterogeneous surface in the presence of an external electric field. Using multiscale analysis, we show that the fast adspecies rapidly reaches a quasi-equilibrium spatial distribution, characterized by a nonequilibrium chemical potential of the fast adspecies. An ordinary differential equation is derived for the time evolution of the nonequilibrium chemical potential. Numerical simulations are performed under different conditions, which confirm the convergence of the dynamics for finite diffusion towards the ultrafast diffusion limit predicted by our multiscale analysis. The numerical simulations also demonstrate that electric fields may induce important diffusive currents on heterogeneous surfaces under the conditions of field emission microscopy.

PACS numbers: 68.43.-h; 82.40.Np; 82.65.+r

I. INTRODUCTION

In natural systems, the time evolution often results from the interplay of several kinetic processes evolving over very different time scales. This is in particular the case in reaction-diffusion systems where the reaction rates as well as the diffusion coefficients may take values ranging over decades depending on the molecular species. It is known that this basic feature contributes to the complexity of reaction-diffusion systems, allowing subsystems to quickly relax to quasi-stationary states which are nevertheless slowly driven by other mechanisms [1–9]. Although the overall system evolves far from equilibrium, some of its parts may remain in self-adjusting quasi-stationary states because the driving mechanisms are much slower than the local relaxation time scales.

An example of such complex systems is provided by the reaction of water formation on rhodium in heterogeneous catalysis [10–12]. Under the conditions of field ion microscopy, the reaction proceeds on a highly heterogeneous medium, which is a metal needle presenting multiple crystalline facets and surrounded by a nonuniform electric field. Such a field deeply influences the surface kinetics as well as the gas mixture of reactants around the catalyst. In this system, the surface diffusion of hydrogen turns out to be much faster than the reaction and the diffusion of oxygen [10–12]. Accordingly, the hydrogen atoms have a fast motion on the surface, quickly leading towards a quasi-equilibrium distribution with a spatial dependence on the local crystalline facets as well as on the electric field. This quasi-equilibrium spatial distribution slowly evolves in time driven by the other kinetic processes taking place on the catalyst over time scales longer than the diffusion of hydrogen.

Such reaction-diffusion processes with multiple time scales and in highly heterogeneous media are common in catalysis as well as in other complex systems. The question arises to find the general principles that determines the quasi-equilibrium spatial distribution and its time evolution.

The purpose of the present paper is to answer this question by performing a multiple scale analysis of the reaction-diffusion equations under the aforementioned conditions. The vehicle of our study is a set of coupled reaction-diffusion partial differential equations which describes a surface process involving the adsorption of several species of reactant molecules from the gas phase, their desorption from the surface, their diffusion until their mutual reaction followed by the desorption of the products. In accordance with the aforementioned situation, one of the adspecies is supposed to have a diffusion on the surface which is ultrafast compared to all the other kinetic processes. The system can be driven out of equilibrium by maintaining, in the gas phase, positive partial pressures for the reactant species and

* Present address: Potsdam Institute for Climate Impact Research, 14412, Potsdam, Germany.
† Present address: Department of Chemical and Biomolecular Engineering, University of Notre Dame, Notre Dame, IN 46556, USA.

a vanishing partial pressure for the product species. In the particular cases where the system reaches a state of thermodynamic equilibrium, the principle of detailed balancing holds between adsorption and desorption as well as for the diffusion of the adspecies present in the system. The reaction-diffusion system we consider is thus compatible with thermodynamic requirements, which allows us to properly define the quasi-equilibrium state once the system is driven out of equilibrium.

The treatment of the coupled reaction-diffusion equations is performed using a multiple scale analysis based on the assumption that the diffusion term of the ultrafast adspecies is much larger than the other terms. Using the theorem of the Fredholm alternative [13], we obtain a great simplification in the resolution of the reaction-diffusion equations because the spatial distribution of the ultrafast adspecies is determined by a vanishing diffusive current density. We infer that the corresponding partial differential equation reduces to an ordinary differential equation for the slow time evolution of the nonequilibrium chemical potential of the ultrafast adspecies. At a given time, this chemical potential characterizes the quasi-equilibrium spatial distribution over the whole surface. The value of this chemical potential is thus common to all the crystalline facets and all the sites that the ultrafast adspecies may occupy on the surface. The validity and efficiency of the method is demonstrated by its comparison with the full numerical integration of the reaction-diffusion equations in the theoretical system here considered.

The paper is organized as follows. The general formulation of problem is set up in Sec. II. The equilibrium and quasi-equilibrium states are presented in Sec. III. The multiple scale analysis is performed in Sec. IV. The numerical results are presented in Sec. V. Conclusions are drawn in Sec. VI.

II. GENERAL FORMULATION

A. The chemical network

We consider a heterogeneous surface upon which two adspecies A and B react and diffuse at rates with some specific spatial dependence. The adspecies are coming from a gas phase above the surface where they exist in monomeric, dimeric, or polymeric form. In the present work, we take a minimal model made up from basic reaction mechanisms. The first processes consist of the adsorption and desorption of adspecies A:

$$\mathrm{A}_m(\mathrm{gas}) \;+\; m\,\emptyset \;\underset{k_{\mathrm{d}}^{\mathrm{A}}}{\overset{k_{\mathrm{a}}^{\mathrm{A}}}{\rightleftharpoons}}\; m\,\mathrm{A(ad)}\,, \tag{1}$$

where we denote by $\mathrm{A}_m(\mathrm{gas})$ as an A_m molecule in the gas phase, A(ad) as an adsorbed particle and $\emptyset$ as an empty site of the surface. The integer m accounts for the order of the reaction. For $m = 1$, the adspecies A is in monomeric form in the gas phase. For $m = 2$, $\mathrm{A}_m(\mathrm{gas})$ will consists of a dimer, in which case the processes in Eq. (1) describe dissociative adsorption and associative desorption. Similarly, we have for adspecies B:

$$\mathrm{B}_n(\mathrm{gas}) \;+\; n\,\emptyset \;\underset{k_{\mathrm{d}}^{\mathrm{B}}}{\overset{k_{\mathrm{a}}^{\mathrm{B}}}{\rightleftharpoons}}\; n\,\mathrm{B(ad)}\,, \tag{2}$$

with another integer n. Once on the surface, the adspecies A and B diffuse at their own hopping rates:

$$\mathrm{A(ad)} \;+\; \emptyset \;\overset{k_{\mathrm{diff}}^{\mathrm{A}}}{\rightleftharpoons}\; \emptyset \;+\; \mathrm{A(ad)}\,, \tag{3}$$

$$\mathrm{B(ad)} \;+\; \emptyset \;\overset{k_{\mathrm{diff}}^{\mathrm{B}}}{\rightleftharpoons}\; \emptyset \;+\; \mathrm{B(ad)}\,. \tag{4}$$

When they meet, the particles A(ad) and B(ad) react together, directly leading to the formation of the product, AB(gas), which immediately desorbs in our model:

$$\mathrm{A(ad)} \;+\; \mathrm{B(ad)} \;\underset{k_{\mathrm{rr}}}{\overset{k_{\mathrm{r}}}{\rightleftharpoons}}\; 2\,\emptyset \;+\; \mathrm{AB(gas)}\,. \tag{5}$$

In the general case where there is a partial pressure of the AB species in the gas phase, the reverse reaction is possible as here assumed.

B. The reaction-diffusion equations

We adopt a mean-field approach where the state of the surface is described by the mean local coverages of both adspecies, $\theta_{\mathrm{A}}(\mathbf{r}, t)$ and $\theta_{\mathrm{B}}(\mathbf{r}, t)$, defined at each point $\mathbf{r}$ of the surface at some time t. The time evolution is thus ruled

by the coupled reaction-diffusion equations:

$$\partial_t \theta_{\rm A} \;=\; \mathcal{R}_{\rm A} - \boldsymbol{\nabla}\cdot\mathbf{J}_{\rm A}\,, \tag{6}$$
$$\partial_t \theta_{\rm B} \;=\; \mathcal{R}_{\rm B} - \boldsymbol{\nabla}\cdot\mathbf{J}_{\rm B}\,, \tag{7}$$

where $\mathcal{R}_{\rm A}$ and $\mathcal{R}_{\rm B}$ are functions accounting for the contribution of reaction processes to the coverage dynamics of adspecies A and B. On the other hand, $\mathbf{J}_{\rm A}$ and $\mathbf{J}_{\rm B}$ denote the current densities due to the diffusion of adspecies A and B over the surface, while $(\boldsymbol{\nabla}\cdot)$ denotes the divergence defined on the curved surface. Naturally, the reaction and diffusion terms will depend explicitly on the position variable $\mathbf{r}$ since the surface is heterogeneous.

1. Reaction

Applying the mass action law to the mechanisms (1)-(5), the reaction terms in (6) and (7) read

$$\mathcal{R}_{\rm A} \;=\; m\,k_{\rm a}^{\rm A} P_{{\rm A}_m}\theta_\emptyset^m - m\,k_{\rm d}^{\rm A}\,\theta_{\rm A}^m - k_{\rm r}\,\theta_{\rm A}\,\theta_{\rm B} + k_{\rm rr}\,P_{\rm AB}\,\theta_\emptyset^2\,, \tag{8}$$
$$\mathcal{R}_{\rm B} \;=\; n\,k_{\rm a}^{\rm B} P_{{\rm B}_n}\theta_\emptyset^n - n\,k_{\rm d}^{\rm B}\,\theta_{\rm B}^n - k_{\rm r}\,\theta_{\rm A}\,\theta_{\rm B} + k_{\rm rr}\,P_{\rm AB}\,\theta_\emptyset^2\,, \tag{9}$$

where the mean coverage of empty sites is defined by

$$\theta_\emptyset = 1 - \theta_{\rm A} - \theta_{\rm B}\,. \tag{10}$$

Because of the heterogeneity of the system, all the reaction constants k_j as well as the local partial pressures $P_{\rm X}$ just above the surface may depend on the position $\mathbf{r}$ over the surface by different effects:

(i) Enhancement of partial pressures by the local electric field: Under the conditions of field emission microscopy, there is a high electric field perpendicular to the surface which varies from point to point. Supposing that the surface is a paraboloid of equation $z = (R^2 - x^2 - y^2)/(2R)$ where R is the radius of curvature at the apex, the intensity of the electric field at the surface varies as $F = F_0/\sqrt{1 + (x^2+y^2)/R^2}$ where F_0 is its value at the apex. Since the molecules in the gas phase have an electric polarizability and may also have an electric dipole, the local pressure in the electric field at the surface is enhanced with respect to the pressure far from the surface where the electric field is vanishing. The enhancement of the pressure can be shown to be approximately described by an effective polarizability $\alpha_{\rm X}$ of the species X in the gas phase according to

$$P_{\rm X}(F) = P_{\rm X}(0)\,\mathrm{e}^{\beta\alpha_{\rm X}F^2/2} \qquad \text{with} \quad {\rm X} = {\rm A}_m, {\rm B}_n, {\rm AB}\,, \tag{11}$$

with the inverse temperature $\beta = (kT)^{-1}$ [14].

(ii) Dependence of activation energies on the local electric field: The electric field may also affect the activation energies of the different reactions. In general, the activation energies may have a nonlinear dependence on the intensity of the electric field but this dependence may be supposed to remain linear if the intensity is small enough. The reaction constants are here assumed to have an Arrhenius dependence on the activation energies

$$k_j = k_j^0\,\mathrm{e}^{-\beta(E_j - F d_j)}\,, \tag{12}$$

where k_j^0 is a prefactor specifying the attempt frequency of an event of type j, E_j the corresponding activation energy at zero electric field, and d_j the coefficient of linear response of the barrier on the electric field, which can be interpreted as an effective electric dipole. The prefactor k_j^0 could also depend on the electric field but it is here supposed that the main dependence comes from the effective electric dipole. In particular, for many adsorption processes the activation energy is negligible and may be taken equal to zero.

(iii) Heterogeneous surface orientation on multifaceted crystals: A further possible source of heterogeneity is the anisotropy of the properties of a crystalline surface. Since the underlying solid is a crystal, the different points of the surface correspond to different crystalline orientations which are labelled by Miller indices (h, k, l). It is known that properties such as the activation energies E_j, the prefactors k_j^0, or the dipole coefficients d_j depend on the orientation of the crystalline surface and thus on the location $\mathbf{r}$ at the surface [10–12].

We mention that only the effects *(i)* and *(ii)* will be examined in the present paper.

2. Diffusion

Using a linear-response assumption, the current densities of the diffusing adspecies are in general given by [15]

$$\mathbf{J}_{\rm A} \;=\; -\mathbf{L}_{\rm AA}\cdot\boldsymbol{\nabla}\left(\beta\mu_{\rm A}\right) - \mathbf{L}_{\rm AB}\cdot\boldsymbol{\nabla}\left(\beta\mu_{\rm B}\right)\,, \tag{13}$$
$$\mathbf{J}_{\rm B} \;=\; -\mathbf{L}_{\rm BA}\cdot\boldsymbol{\nabla}\left(\beta\mu_{\rm A}\right) - \mathbf{L}_{\rm BB}\cdot\boldsymbol{\nabla}\left(\beta\mu_{\rm B}\right)\,, \tag{14}$$

in terms of the linear-response coefficients and the chemical potentials obtained by varying the free energy with respect to the partial coverages of both adspecies:

$$\mu_{\rm A} = \frac{\delta \mathcal{F}}{\delta \theta_{\rm A}} \,, \qquad \mu_{\rm B} = \frac{\delta \mathcal{F}}{\delta \theta_{\rm B}} \,. \tag{15}$$

Accordingly, the current densities will vanish at equilibrium where the free energy reaches its minimum value. The linear-response coefficients form tensors, which accounts for possible anisotropies in the diffusion of adspecies on the surface [16]. These tensors may also depend on the partial coverages as well as on space in a heterogeneous medium. In general, they obey Onsager's reciprocity relations, $\mathsf{L}_{\rm AB} = \mathsf{L}_{\rm BA}^{\rm T}$, as a consequence of microreversibility [15].

Neglecting the influence of lateral interactions and supposing that the surface is composed of sites which are either empty $\emptyset$ or occupied by the particles of adspecies A or B, the free energy can be taken of the form

$$\mathcal{F} = \mathcal{E} - \beta^{-1} \mathcal{S} \,, \tag{16}$$

with the energy

$$\mathcal{E} = \int (\varepsilon_{\rm A}\, \theta_{\rm A} + \varepsilon_{\rm B}\, \theta_{\rm B})\, d\mathbf{r} \,, \tag{17}$$

where $\varepsilon_{\rm A}$ and $\varepsilon_{\rm B}$ are the binding energies per site, and the dimensionless entropy

$$\mathcal{S} = - \int [\theta_{\rm A} \ln \theta_{\rm A} + \theta_{\rm B} \ln \theta_{\rm B} + (1 - \theta_{\rm A} - \theta_{\rm B}) \ln(1 - \theta_{\rm A} - \theta_{\rm B})]\, d\mathbf{r} \,, \tag{18}$$

allowing for the three possible states $\{\emptyset, {\rm A}, {\rm B}\}$ of each site. As the consequence of Eq. (15), the chemical potentials are given by

$$\mu_{\rm A} \;=\; \varepsilon_{\rm A} + \beta^{-1} \ln \frac{\theta_{\rm A}}{1 - \theta_{\rm A} - \theta_{\rm B}} \,, \tag{19}$$

$$\mu_{\rm B} \;=\; \varepsilon_{\rm B} + \beta^{-1} \ln \frac{\theta_{\rm B}}{1 - \theta_{\rm A} - \theta_{\rm B}} \,. \tag{20}$$

We remark that these relations hold in equilibrium as well as away from equilibrium as long as local equilibrium is maintained [15].

We consider the case where the coupling between the transports of both adspecies is negligeable $\mathsf{L}_{\rm AB} = 0$ and use the notation $\mathsf{L}_{\rm A} \equiv \mathsf{L}_{\rm AA}$ [12]. Substituting the expression for the chemical potential of adspecies A into the corresponding current density, the latter becomes [10–12, 17–19]:

$$\mathbf{J}_{\rm A} = -\mathsf{D}_{\rm A} \cdot [(1 - \theta_{\rm B})\, \boldsymbol{\nabla} \theta_{\rm A} + \theta_{\rm A}\, \boldsymbol{\nabla} \theta_{\rm B} + \theta_{\rm A} (1 - \theta_{\rm A} - \theta_{\rm B})\, \boldsymbol{\nabla} (\beta \varepsilon_{\rm A})] \,, \tag{21}$$

where the last term accounts for possible heterogeneities in the local binding energy and where the diffusion tensor is defined as

$$\mathsf{D}_{\rm A} \equiv \frac{\mathsf{L}_{\rm A}}{\theta_{\rm A}(1 - \theta_{\rm A} - \theta_{\rm B})} \,. \tag{22}$$

A similar expression holds for the diffusive current density of adspecies B.

III. EQUILIBRIA AND QUASI-EQUILIBRIA

A. Partial equilibria

Let us suppose for a while that the gas phase above the surface only contains the species A_m, in which case the partial pressures of species B_n and AB are vanishing, $P_{\mathrm{B}_n} = P_{\rm AB} = 0$. The only processes happening in the system are the adsorption and desorption of species A_m according to Eq. (1). The time evolution of this system is ruled by the sole reaction-diffusion equation (6) with $\theta_{\rm B} = 0$. If the surface is initially empty, its coverage by adspecies A will grow until the state of thermodynamic equilibrium is reached where the adlayer of particles A is in equilibrium with the gas pressure $0 < P_{\mathrm{A}_m} < \infty$. The state of thermodynamic equilibrium is characterized by the principle of detailed

balancing according to which each process is balanced by its reversal. Consequently, in the presence of the sole species A_m, the adsorption should be balanced by desorption and the current density should vanish at equilibrium:

$$k_{\rm a}^{\rm A} P_{{\rm A}_m} \theta_\emptyset^m = k_{\rm d}^{\rm A}\, \theta_{\rm A}^m \,, \tag{23}$$

$$\mathbf{J}_{\rm A} = 0 \,, \tag{24}$$

with $\theta_\emptyset = 1 - \theta_{\rm A}$. The first condition shows that the coverage should be given by

$$\theta_{\rm A} = \frac{1}{1 + \left(\frac{k_{\rm d}^{\rm A}}{k_{\rm a}^{\rm A} P_{{\rm A}_m}}\right)^{\frac{1}{m}}} \,, \tag{25}$$

while the second condition leads to the following form obtained by the thermodynamic condition that the free energy (16)-(18) should reach its minimum value at equilibrium:

$$\theta_{\rm A} = \frac{1}{1 + {\rm e}^{\beta\left(\varepsilon_{\rm A} - \mu_{\rm A}^{\rm eq}\right)}} \,, \tag{26}$$

where the equilibrium chemical potential $\mu_{\rm A}^{\rm eq}$ is uniform.

Clearly, both expressions (25) and (26) have to coincide. Now, in a heterogeneous medium, we may expect a spatial dependence of the quantities $P_{{\rm A}_m}(\mathbf{r})$, $k_{\rm a}^{\rm A}(\mathbf{r})$, $k_{\rm d}^{\rm A}(\mathbf{r})$, and $\varepsilon_{\rm A}(\mathbf{r})$. Consequently, the spatial dependence of the latter can be deduced from the knowledge of the former quantities by

$$\varepsilon_{\rm A}(\mathbf{r}) = \frac{1}{m\beta} \ln \frac{k_{\rm d}^{\rm A}(\mathbf{r})}{k_{\rm a}^{\rm A}(\mathbf{r}) P_{{\rm A}_m}(\mathbf{r})} + \mu_{\rm A}^{\rm eq} \,. \tag{27}$$

The same principle concerns the adspecies B so that we also infer that

$$\varepsilon_{\rm B}(\mathbf{r}) = \frac{1}{n\beta} \ln \frac{k_{\rm d}^{\rm B}(\mathbf{r})}{k_{\rm a}^{\rm B}(\mathbf{r}) P_{{\rm B}_n}(\mathbf{r})} + \mu_{\rm B}^{\rm eq} \,. \tag{28}$$

We notice that these expressions for the local binding energies can now be used under possible nonequilibrium general conditions. In particular, the current density of particles A given by Eqs. (21)-(22) can be written in the equivalent form

$$\mathbf{J}_{\rm A} = -\mathbf{L}_{\rm A} \cdot \boldsymbol{\nabla} \Phi_{\rm A} \,, \tag{29}$$

with the potential

$$\Phi_{\rm A} \equiv \beta \mu_{\rm A} = \ln \left[\left(\frac{k_{\rm d}^{\rm A}}{k_{\rm a}^{\rm A} P_{{\rm A}_m}} \right)^{\frac{1}{m}} \frac{\theta_{\rm A}}{1 - \theta_{\rm A} - \theta_{\rm B}} \right] + \beta \mu_{\rm A}^{\rm eq} \,, \tag{30}$$

obtained by combining Eqs. (19) and (27).

B. Complete equilibrium

Let us suppose that the surface is in contact with a gas phase with partial pressures of all the species A_m, B_n, and AB. In this general case, all the processes of adsorption, desorption and reaction are active on the surface. After a long enough relaxation time, the system is expected to reach the state of *complete* thermodynamic equilibrium, which is characterized by the detailed balancing of every adsorption, desorption, and reaction process, so that every one of the following conditions should be simultaneously satisfied:

$$k_{\rm a}^{\rm A} P_{{\rm A}_m} \theta_\emptyset^m = k_{\rm d}^{\rm A}\, \theta_{\rm A}^m \,, \tag{31}$$

$$k_{\rm a}^{\rm B} P_{{\rm B}_n} \theta_\emptyset^n = k_{\rm d}^{\rm B}\, \theta_{\rm B}^n \,, \tag{32}$$

$$k_{\rm r}\, \theta_{\rm A}\, \theta_{\rm B} = k_{\rm rr}\, P_{\rm AB}\, \theta_\emptyset^2 \,, \tag{33}$$

$$\mathbf{J}_{\rm A} = 0 \,, \tag{34}$$

$$\mathbf{J}_{\rm B} = 0 \,, \tag{35}$$

with $\theta_\emptyset = 1 - \theta_{\rm A} - \theta_{\rm B}$. All these conditions cannot simultaneously hold unless the partial pressures satisfy the constraint that

$$P_{\rm AB} = \frac{k_{\rm r}}{k_{\rm rr}} \left(\frac{k_{\rm a}^{\rm A} P_{{\rm A}_m}}{k_{\rm d}^{\rm A}} \right)^{\frac{1}{m}} \left(\frac{k_{\rm a}^{\rm B} P_{{\rm B}_n}}{k_{\rm d}^{\rm B}} \right)^{\frac{1}{n}} , \tag{36}$$

which is nothing else than the state of chemical equilibrium where the partial pressures are fixed by

$$\frac{P_{\rm AB}}{P_{{\rm A}_m}^{\frac{1}{m}} P_{{\rm B}_n}^{\frac{1}{n}}} = K_{\rm eq} , \tag{37}$$

in terms of the equilibrium constant $K_{\rm eq}$ of the overall reaction $m^{-1}{\rm A}_m + n^{-1}{\rm B}_n \rightleftharpoons {\rm AB}$.

If the partial pressure of the product species AB is vanishing $P_{\rm AB} = 0$, the system cannot reach the state of complete equilibrium unless either $P_{{\rm A}_m} = 0$ or $P_{{\rm B}_n} = 0$, which are the states of partial equilibrium mentioned in the previous subsection. If $P_{\rm AB} = 0$, $P_{{\rm A}_m} > 0$, and $P_{{\rm B}_n} > 0$, the reaction proceeds on the surface without reaching any equilibrium so that the system remains in a nonequilibrium state, possibly reaching a nonequilibrium steady state after a long enough relaxation time.

C. Quasi-equilibria

In the case where one of the five processes corresponding to the detailed balancing conditions (31)-(35) is faster than all the four other processes, the system may reach a state of quasi-equilibrium over a time scale longer than the characteristic time of the fast process but shorter than the relaxation time of complete equilibrium.

For the following, we consider the case of ultrafast diffusion of adspecies A. Thanks to their ultrafast diffusion on the surface, the particles A soon reach a spatial distribution where the current density of adspecies A is vanishing,

$$\mathbf{J}_{\rm A} = -\mathsf{L}_{\rm A} \cdot \boldsymbol{\nabla} \Phi_{\rm A} = 0 , \tag{38}$$

so that the potential, $\Phi_{\rm A} = \beta \mu_{\rm A}$, becomes uniform. If the system is isothermal (i.e., if heat conduction is fast enough), this condition requires the uniformity of the chemical potential, $\boldsymbol{\nabla} \mu_{\rm A} = 0$. Using Eq. (19), we conclude that the current density should vanish if the partial coverage of adspecies A takes the form:

$$\theta_{\rm A}(\mathbf{r}, t) = \frac{1 - \theta_{\rm B}(\mathbf{r}, t)}{1 + {\rm e}^{\beta[\varepsilon_{\rm A}(\mathbf{r}) - \mu_{\rm A}(t)]}} , \tag{39}$$

We notice that this partial coverage is not necessarily uniform because of heterogeneities in the local binding energy $\varepsilon_{\rm A}(\mathbf{r})$ and the possible spatial variations of the other partial coverage $\theta_{\rm B}(\mathbf{r}, t)$. A key point is that the sole condition for the vanishing of the current density is the uniformity of the chemical potential $\mu_{\rm A}(t)$, which may thus still depend on time as long as the complete thermodynamic equilibrium has not yet been reached. In this sense, Eq. (39) describes the state of quasi-equilibrium for the spatial distribution of adspecies A with respect to the diffusion of particles A.

IV. MULTIPLE SCALE ANALYSIS

The main question addressed in the present paper is to understand the time evolution of the quasi-equilibrium distribution (39) and, in particular, the nonequilibrium chemical potential $\mu_{\rm A}(t)$. To answer this question, we carry out a multiple scale analysis.

A. Expansion in perturbation series

According to the assumption of ultrafast diffusion of adspecies A, the diffusion coefficients $\mathbf{D}_{\rm A}$ determine a time scale that is shorter than the other competing processes. Consequently, the diffusion term $(-\boldsymbol{\nabla} \cdot \mathbf{J}_{\rm A})$ dominates in the reaction-diffusion equations (6)-(7). This feature can be expressed by introducing a fictitious parameter ϵ which is supposed to be very small but set equal to unity at the end of the analysis. The reaction-diffusion equations can thus be written in the form

$$\partial_t \theta_{\rm A} = \mathcal{S}_{\rm A} - \frac{1}{\epsilon} \boldsymbol{\nabla} \cdot \mathbf{J}_{\rm A} , \tag{40}$$

$$\partial_t \theta_{\rm B} = \mathcal{S}_{\rm B} , \tag{41}$$

where $\mathcal{S}_\mathrm{A} \equiv \mathcal{R}_\mathrm{A}$ and $\mathcal{S}_\mathrm{B} \equiv \mathcal{R}_\mathrm{B} - \boldsymbol{\nabla}\cdot\mathbf{J}_\mathrm{B}$ denote the rates of the slow processes.

The analysis starts by expanding the partial coverage and the current density of adspecies A in powers of the small parameter ϵ:

$$\theta_\mathrm{A} \equiv \theta \;=\; \theta^{(0)} + \epsilon\,\theta^{(1)} + \epsilon^2\theta^{(2)} + \cdots\,, \tag{42}$$

$$\mathbf{J}_\mathrm{A} \equiv \mathbf{J} \;=\; \mathbf{J}^{(0)} + \epsilon\,\mathbf{J}^{(1)} + \epsilon^2\mathbf{J}^{(2)} + \cdots \tag{43}$$

The index A is omitted unless explicitly written. We will also use the notation

$$\mathbf{J} = -\mathsf{L}\cdot\boldsymbol{\nabla}\Phi\,, \tag{44}$$

with the potential $\Phi = \Phi_\mathrm{A}$ given by Eq. (30).

Substituting the expansions (42)-(43) into the reaction-diffusion (40) for adspecies A, which can be rewritten as

$$\boldsymbol{\nabla}\cdot\mathbf{J} = \epsilon\,(\mathcal{S} - \partial_t\theta)\;, \tag{45}$$

we get at each successive order in powers of ϵ the following equations:

$$O(\epsilon^0): \qquad \boldsymbol{\nabla}\cdot\mathbf{J}^{(0)} \;=\; 0\,, \tag{46}$$

$$O(\epsilon^1): \qquad \boldsymbol{\nabla}\cdot\mathbf{J}^{(1)} \;=\; \mathcal{S}(\theta^{(0)}) - \partial_t\theta^{(0)}\,, \tag{47}$$

$$\vdots$$

with $\mathcal{S} \equiv \mathcal{S}_\mathrm{A} = \mathcal{R}_\mathrm{A}$.

B. Leading order

At the leading order, the current density of adspecies A should satisfy the equation:

$$\boldsymbol{\nabla}\cdot\mathbf{J}^{(0)} = \boldsymbol{\nabla}\cdot\mathbf{J}_\mathrm{A}(\theta_\mathrm{A}^{(0)}, \theta_\mathrm{B}) = 0\,, \tag{48}$$

which is the condition of stationarity for the diffusion equation of the ultrafast adspecies A.

We suppose that the surface is not in contact with particle reservoirs other than the gas phase so that there is no flux of particle A at the boundaries of the domain of the surface where the reaction-diffusion process evolves, whereupon the current density itself should vanish at the leading order:

$$\mathbf{J}^{(0)} = \mathbf{J}_\mathrm{A}(\theta_\mathrm{A}^{(0)}, \theta_\mathrm{B}) = 0\,. \tag{49}$$

As explained in the previous section, the solution $\theta_\mathrm{A}^{(0)}(\mathbf{r}, t)$ at the leading order is therefore the quasi-equilibrium spatial distribution given by Eq. (39) with a time-dependent uniform chemical potential $\mu_\mathrm{A}(t)$.

C. Next-to-leading order

Using the expression (44), the next-to-leading term of the current density is given by

$$\mathbf{J}^{(1)} = -\mathsf{L}(\theta^{(0)})\cdot\boldsymbol{\nabla}\left[\frac{\partial\Phi}{\partial\theta}(\theta^{(0)})\,\theta^{(1)}\right] - \left[\frac{\partial\mathsf{L}}{\partial\theta}(\theta^{(0)})\cdot\underbrace{\boldsymbol{\nabla}\Phi(\theta^{(0)})}_{=0}\right]\theta^{(1)}\,. \tag{50}$$

The second term is zero because the leading-order solution $\theta^{(0)}$ is the quasi-equilibrium distribution (39) such that the dimensionless chemical potential Φ is uniform and its gradient vanishes, $\boldsymbol{\nabla}\Phi(\theta^{(0)}) = 0$.

Accordingly, the next-to-leading equation (47) becomes

$$\boldsymbol{\nabla}\cdot\left\{\mathsf{L}(\theta^{(0)})\cdot\boldsymbol{\nabla}\left[\Phi'(\theta^{(0)})\,\theta^{(1)}\right]\right\} = \partial_t\theta^{(0)} - \mathcal{S}(\theta^{(0)})\,, \qquad \text{with} \quad \Phi' \equiv \frac{\partial\Phi}{\partial\theta}\,, \tag{51}$$

which is an inhomogeneous linear partial differential equation for the perturbation $\theta^{(1)}$ to the quasi-equilibrium coverage $\theta^{(0)}$:

$$\hat{\mathcal{L}}\,\theta^{(1)} = q^{(0)}\,, \tag{52}$$

with the linear operator

$$\hat{\mathcal{L}}\, f = \boldsymbol{\nabla} \cdot \Big\{ \mathbf{L}(\theta^{(0)}) \cdot \boldsymbol{\nabla} \Big[\Phi'(\theta^{(0)})\, f \Big] \Big\} \,, \tag{53}$$

and $q^{(0)} = \partial_t \theta^{(0)} - \mathcal{S}(\theta^{(0)})$. One can obtain the adjoint of $\hat{\mathcal{L}}$ by evaluating its elements between the two functions f and g in Hilbert space and integrating by parts twice, to get

$$\hat{\mathcal{L}}^\dagger\, g = \Phi'(\theta^{(0)})\, \boldsymbol{\nabla} \cdot \Big[\mathbf{L}(\theta^{(0)})^{\mathrm{T}} \cdot \boldsymbol{\nabla}\, g \Big] \,, \tag{54}$$

where T denotes the transpose of the linear-response matrix.

Now, solving the inhomogeneous linear equation (52) requires first to determine the null space of zero eigenvalue for the linear operator and its adjoint. For no-flux boundary conditions, the null eigensolution of $\hat{\mathcal{L}}$ is of the form:

$$f = \frac{a}{\Phi'(\theta^{(0)})} \,, \qquad \text{such that} \quad \hat{\mathcal{L}}\, f = 0 \,, \tag{55}$$

while the null eigensolution of the adjoint operator is given by

$$g = b \,, \qquad \text{such that} \quad \hat{\mathcal{L}}^\dagger\, g = 0 \,, \tag{56}$$

where a and b are constants independent of both space and time.

Since $\hat{\mathcal{L}}$ has a zero eigenvalue, one must invoke the theorem of the Fredholm alternative [13]. Accordingly, the inhomogeneous linear equation (52) will admit a solution under the solvability condition that its right-hand side $q^{(0)}$ is orthogonal to the null eigenspace of $\hat{\mathcal{L}}^\dagger$:

$$\int d\mathbf{r}\, g^*\, q^{(0)} = 0 \,. \tag{57}$$

Since the null eigensolution g is constant (i.e., uniform), we find that

$$\int d\mathbf{r} \Big[\partial_t \theta^{(0)} - \mathcal{S}(\theta^{(0)}) \Big] = 0 \,. \tag{58}$$

Using the expression (39) for $\theta^{(0)} = \theta_{\mathrm{A}}^{(0)}$ as well as the second reaction-diffusion equation (41), the solvability condition (58) gives us the time evolution of the nonequilibrium chemical potential $\mu_{\mathrm{A}}(t)$ of the quasi-equilibrium distribution (39) as

$$\frac{d\mu_{\mathrm{A}}}{dt} = \frac{\int w \Big[(1-\theta_{\mathrm{B}})\, \mathcal{S}_{\mathrm{A}}(\theta_{\mathrm{A}}^{(0)}, \theta_{\mathrm{B}}) + \theta_{\mathrm{A}}^{(0)}\, \mathcal{S}_{\mathrm{B}}(\theta_{\mathrm{A}}^{(0)}, \theta_{\mathrm{B}}) \Big]\, d\mathbf{r}}{\beta \int w\, \theta_{\mathrm{A}}^{(0)} (1 - \theta_{\mathrm{A}}^{(0)} - \theta_{\mathrm{B}})\, d\mathbf{r}} \,, \tag{59}$$

with the weight

$$w = \frac{1}{1-\theta_{\mathrm{B}}} \,, \tag{60}$$

which is the central result of this paper.

Once the solvability condition is satisfied, the perturbation $\theta^{(1)} = \theta_{\mathrm{A}}^{(1)}$ can be obtained which is the solution of the next-to-leading equation (47) and which determines the nonvanishing current (50) of particles A induced on the surface by the slow processes going on as long as the surface remains out of equilibrium:

$$\mathbf{J}_{\mathrm{A}} = -\epsilon\, \mathbf{D}_{\mathrm{A}}(\theta_{\mathrm{A}}^{(0)}, \theta_{\mathrm{B}}) \cdot \Big[(1-\theta_{\mathrm{B}})\, \boldsymbol{\nabla} \theta_{\mathrm{A}}^{(1)} + \theta_{\mathrm{A}}^{(1)}\, \boldsymbol{\nabla} \theta_{\mathrm{B}} + \theta_{\mathrm{A}}^{(1)} (1 - 2\theta_{\mathrm{A}}^{(0)} - \theta_{\mathrm{B}})\, \boldsymbol{\nabla} (\beta \varepsilon_{\mathrm{A}}) \Big] + O(\epsilon^2) \,, \tag{61}$$

where the quasi-equilibrium condition $\boldsymbol{\nabla} \Phi(\theta_{\mathrm{A}}^{(0)}, \theta_{\mathrm{B}}) = 0$ has been used.

In summary, if the diffusion of adspecies A is ultrafast, the time evolution of the system is ruled by the partial differential equation (41) for the partial coverage of adspecies B which is coupled to the ordinary differential equation (59) with the weight (60), while the partial coverage of adspecies A is determined at each time step by the quasi-equilibrium distribution (39).

V. NUMERICAL RESULTS

A. Geometry of the surface

Here, we suppose that the surface is a revolution paraboloid, as often done for field-emitter tips [10–12, 20]. Therefore, the description of the system can be carried out in terms of the parabolic coordinates:

$$x = \sqrt{R\,\eta}\,\cos\varphi\,, \tag{62}$$

$$y = \sqrt{R\,\eta}\,\sin\varphi\,, \tag{63}$$

$$z = \frac{1}{2}(R-\eta)\,, \tag{64}$$

with $0 \leq \eta < +\infty$ and $0 \leq \varphi < 2\pi$ [21]. As depicted in Fig. 1, the paraboloid has a cylindrical symmetry around the z axis and extends to negative values of z. Its apex is located at $x = y = 0$ and $z = R/2$ where the radius of curvature is equal to R.

An element of surface area is given by $d\mathbf{r} = d^2r = \rho\,d\varphi\,ds$, where $\rho = \sqrt{R\,\eta}$ is the radial distance between the axis of cylindrical symmetry and the point (η, φ) of the paraboloid, while ds is an arc element of the radial parabola $\rho = \sqrt{R^2 - Rz}$ composing the paraboloid:

$$ds = \sqrt{1 + \left(\frac{d\rho}{dz}\right)^2}\,dz = \sqrt{1 + \frac{R}{\eta}}\,\frac{d\eta}{2}\,. \tag{65}$$

Consequently, the element of surface area is expressed in parabolic coordinates as

$$d\mathbf{r} = d^2r = R\sqrt{1 + \frac{\eta}{R}}\,d\eta\,d\varphi\,. \tag{66}$$

For the sake of simplicity, we shall assume that the heterogeneity has the cylindrical symmetry of the paraboloid so that all the space-dependent features of the system will be specified in terms of the variable η, exclusively. In particular, the magnitude of the electric field at the tip's surface will be given by

$$F = \frac{F_0}{\sqrt{1 + \frac{\eta}{R}}}\,. \tag{67}$$

In this respect, the tip surface is partitioned into a set of rings at constant values of the coordinate η and extending over an interval $d\eta$. The arc of perimeter of each ring takes the value:

$$P = \int_0^{2\pi} \rho\,d\varphi = 2\pi\sqrt{R\,\eta}\,, \tag{68}$$

and its surface area is given by

$$dA = P\,ds = \pi R\,\sqrt{1 + \frac{\eta}{R}}\,d\eta\,. \tag{69}$$

The natural unit of length is the radius of curvature R of the tip.

B. General assumptions of the numerical simulations

For numerical purposes, we proceed to a discretization of the surface geometry into a set of N rings. The partial coverages are evaluated in the middle of each ring at the positions

$$\eta_i = i\,\Delta\eta \qquad (i = 0, 1, 2, ..., N-1)\,. \tag{70}$$

The discretization of the reaction-diffusion evolution equations is carried out in Appendix A, as well as the corresponding multiscale analysis in the limit of ultrafast diffusion.

In all cases, we shall focus on the evolution of the coverage of adspecies A as a function of its diffusion coefficient D_{A}. Our purpose is to test the validity of the results of the multiscale analysis in the ultrafast diffusion limit. We

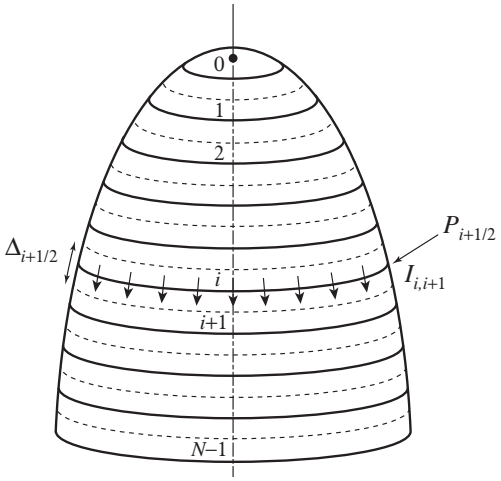

FIG. 1: Schematic illustration of the discretization of a paraboloid in terms of N rings. The middle of each ring i is positioned at $\eta_i = i\Delta\eta$ (dashed lines), the apex being at $i = 0$. Their boundaries are located at $\eta_{i+1/2} = \eta_i + \Delta\eta/2$ (solid lines), they have the perimeters $P_{i+1/2}$, and they are crossed by the current or flux $I_{i,i+1}$ of adspecies defined by Eq. (A5). The distance between the middles of the rings i and $i+1$ is denoted $\Delta_{i+1/2}$.

will compare the solutions of the reaction-diffusion equations (6)-(7) with the coverage evolution as described by the quasi-equilibrium approach based on Eq. (59). The latter is carried out using both, the exact expression for the weight, as provided by Eq. (60), and the approximation $w = 1$ used elsewhere [10–12].

As an initial distribution for adspecies A, we shall consider the equilibrium one as given by Eq. (39) with $\mu_{\rm A} = \mu_{\rm A}^{\rm eq}$. Furthermore, we consider two kinds of initial distributions for adspecies B: a homogeneous and an inhomogeneous one. In the former case, we assume all the rings have an initial coverage of 1/2 ML. For the later, we consider the initial coverage of adspecies B as gradually diminishing from 1/2 monolayer (ML) at the apex (corresponding to $i = 0$) to zero at the flanks of the tip (for $i = N - 1$), according to:

$$\theta_{\rm B} = \frac{1}{2}\left(1 - \frac{i}{N-1}\right) \qquad (i = 0, 1, 2, ..., N-1)\,. \tag{71}$$

Moreover, the evolution of the adspecies B is simplified by neglecting its adsorption, desorption and diffusion, in which case the processes (2) and (4) are absent of the chemical network. The partial pressure of the product species is always vanishing, $P_{\rm AB} = 0$. The evolution equation of the adspecies B is thus given by

$$\partial_t \theta_{\rm B} = -k_{\rm r}\theta_{\rm A}\theta_{\rm B}\,, \tag{72}$$

If the reaction rate vanishes, $k_{\rm r} = 0$, the coverage of adspecies B remains constant in time at its initial value.

In the following, we consider four different models whenever the reaction rate and the external electric field are vanishing or not. The values of the parameters of these four models are given in Table I.

C. The system in the absence of reaction

We first consider the system in the absence of reaction, $k_{\rm r} = 0$, so that the coverage of adspecies B keeps its initial value during the whole time evolution.

1. Model I: The unreactive system in the absence of electric field

If the external electric field is vanishing, $F = 0$, all the rate constants are everywhere equal on the surface and there is no contribution of the local energy potential to the diffusive current, $\boldsymbol{\nabla}\varepsilon_{\rm A} = 0$.

If the species $\rm A_m$ is monomeric, $m = 1$, the reaction rate (8) is linear in the coverage $\theta_{\rm A}$. Starting from the quasi-equilibrium coverage (39) as an initial condition, the solution of the reaction-diffusion equation remains in the

Models	I	II	III	IV
F (V/nm)	0	10	0	10
$k_{\rm a}^{\rm A}$ ($\rm s^{-1}$)	1	1	1	1
$\alpha_{{\rm A}_m}$ (eV $\rm nm^2$ $\rm V^{-2}$)	1×10^{-3}	1×10^{-3}	1×10^{-3}	1×10^{-3}
$k_{\rm d}^{\rm A0}$ ($\rm s^{-1}$)	1×10^{10}	1×10^{10}	1×10^{10}	1×10^{10}
$E_{\rm d}^{\rm A}$ (eV)	1.0	1.0	1.0	1.0
$d_{\rm d}^{\rm A}$ (eV nm $\rm V^{-1}$)	0.02	0.02	0.02	0.02
$k_{\rm r}^{0}$ ($\rm s^{-1}$)	0	0	1×10^{10}	1×10^{10}
$E_{\rm r}$ (eV)	0	0	0.7	0.7
$d_{\rm r}$ (eV nm $\rm V^{-1}$)	0	0	0.01	0.01

TABLE I: Sets of parameters associated with the different models under scope. In all models, we assume $R = 1$, $T = 350$ K and $P_{\rm A}(0) = 100$ (in units setting $k_{\rm a}^{\rm A} = 1$). Since the Boltzmann constant takes the value $k = 8.617\times10^{-5}$ eV/K, the inverse temperature is given by $\beta = (kT)^{-1} = 33.2$ $\rm eV^{-1}$. Except if otherwise explicitly mentioned, we set $\mu_{\rm A}^{\rm eq} = -0.5$ eV and $\mu_{\rm A}(t=0) = -1.5$ eV. We notice that $k_{\rm d}^{\rm A} = k_{\rm d}^{\rm A0}\exp\left[-\beta(E_{\rm d}^{\rm A} - Fd_{\rm d}^{\rm A})\right]$ according to Eq. (12).

factorized form

$$\theta_{\rm A} = C(t)\,[1-\theta_{\rm B}(\mathbf{r})] \qquad \text{with} \quad C(t) = \frac{1}{1+{\rm e}^{\beta[\varepsilon_{\rm A}-\mu_{\rm A}(t)]}}\,, \tag{73}$$

with a spatial dependence fixed by the coverage of adspecies B multiplied by a time-dependent coefficient, $C(t)$. Indeed, the current density vanishes for this quasi-equilibrium coverage and the reaction-diffusion equation (6) reduces to

$$\frac{dC}{dt} = k_{\rm a}^{\rm A}P_{\rm A} - \left(k_{\rm a}^{\rm A}P_{\rm A} + k_{\rm d}^{\rm A}\right)C\,, \tag{74}$$

which is an ordinary differential equation without any spatial dependence in the case where $F = 0$ and $k_{\rm r} = 0$. Consequently, the coverage of adspecies A converges to its asymptotic value,

$$\lim_{t\to\infty}\theta_{\rm A} = \frac{1-\theta_{\rm B}}{1+\frac{k_{\rm d}^{\rm A}}{k_{\rm a}^{\rm A}P_{\rm A}}}\,, \tag{75}$$

at the same rate everywhere on the surface. In this special case, we thus expect the same behavior for different values of the diffusion coefficient $D_{\rm A}$, whether finite or infinite.

This is indeed confirmed by numerical simulations for the homogeneous coverage of adspecies B at 1/2 ML (see Fig. 2). Under the conditions we consider, the reaction-diffusion equation reduces to the same equation on all the rings. Therefore, the evolution of adspecies A is space independent, consisting of a monotonic increase towards the asymptotic value (75) given by $\lim_{t\to\infty}\theta_{\rm A} \simeq 1/2$ ML, according to the parameter values of Table I. Moreover, we see in Fig. 2 that all the curves obtained for different values of the diffusion coefficient $D_{\rm A}$, as well as the infinite-diffusion curve, collapse to the same curve, confirming the independence on diffusion in the case of linear adsorption-desorption kinetics ($m = 1$).

Naturally, one might expect a different situation when the distribution of adspecies B is an inhomogeneous one. Figure 3 depicts the plot of the dynamics of $\theta_{\rm A}$ for different rings, whose coverage distribution of adspecies B is given by Eq. (71). From bottom to top, the curves in this figure correspond to rings situated between the apex and the flanks, showing the spatial dependence expected from Eq. (73). Here also, the plot includes the curves that result from taking distinct values of $D_{\rm A}$. In spite of the spatial inhomogeneity introduced by the coverage (71) of adspecies B, no dependence on the diffusion coefficient is observed as the curves corresponding to a same ring are identical regardless the value of $D_{\rm A}$, as expected for the factorized form (73).

On the other hand, a different behavior arises if the initial distribution of adspecies A is not the quasi-equilibrium one given by Eq. (39), in which case the kinetics is influenced by the diffusion rate (not shown). In other words, if the initial coverage distribution of adspecies A is in quasi-equilibrium, then the system continues to evolve under quasi-equilibrium conditions in the absence of an electric field. This is a consequence of the linear character of the adsorption-desorption terms in Eq. (8) since we have assumed $m = 1$. Indeed, if the reaction rate $\mathcal{R}_{\rm A}$ is linear, then the reaction-diffusion equation (6) admits solutions with space and time uncoupled if $F = 0$ so that, whenever the diffusion rate $(-\boldsymbol{\nabla}\cdot\mathbf{J}_{\rm A})$ is initially zero, it remains so throughout the transient process.

In contrast, when the adspecies A undergoes dissociative adsorption and associative desorption ($m = 2$), differences appear in the coverage dynamics when considering different values of $D_{\rm A}$. This is shown in Fig. 4, for the same initial

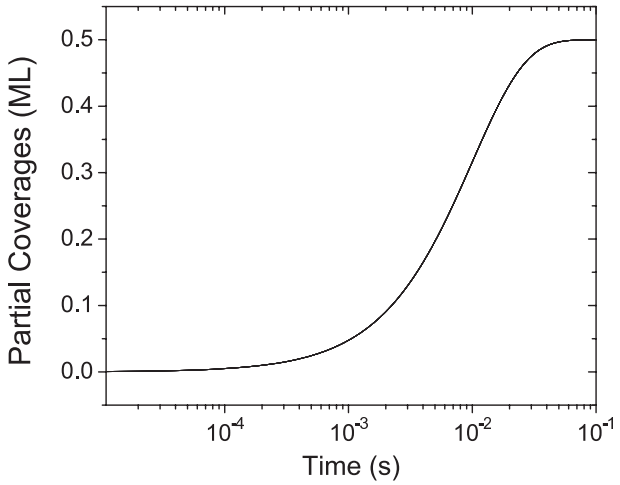

FIG. 2: The partial coverage build-up curves for adspecies A on all the rings of a field emitter tip for the monomeric case ($m = 1$) in the absence of both the A+B reaction and an electric field, with an initial homogeneous distribution for adspecies B ($\theta_{\rm B} = 0.5$ ML). This plot includes curves obtained for $D_{\rm A}/R^2 = 10^{\gamma}$ s^{-1}, with $\gamma = 1, 2, 3, 4$, as well as the corresponding infinite-diffusion case. Notice that all the curves completely overlap. Parameters: $k_{\rm a}^{\rm A} = 1$ s^{-1}, $k_{\rm d}^{\rm A0} = 1 \times 10^{10}$ s^{-1}, $E_{\rm d}^{\rm A} = 1$ eV, $T = 350$ K and $P_{\rm A}(0) = 100$ (in units setting $k_{\rm a}^{\rm A} = 1$), $\mu_{\rm A}^{\rm eq} = -0.5$ eV, and $\mu_{\rm A}(t = 0) = -1.5$ eV (see Model I in Table I).

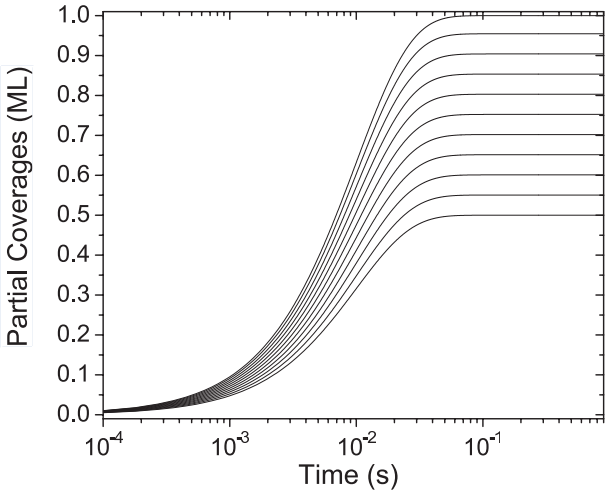

FIG. 3: The partial coverage build-up curves for adspecies A on rings $i = 2, 10, 20, \ldots, 100$ (ring $i = 2$ curve at the bottom) for the monomeric case ($m = 1$) in the absence of both the A+B reaction and an electric field, with an inhomogeneous distribution for adspecies B given by Eq. (71). Similarly, as in Fig. 2, this plot exhibits overlapping curves for $D_{\rm A}/R^2 = 10^{\gamma}$ s^{-1}, with $\gamma = 1, 2, 3, 4$, as well as for $D_{\rm A} = \infty$. Same parameters as in Fig. 2 (Model I in Table I) .

coverage distributions as taken in Fig. 3. In this case, during the transient regime towards equilibrium, the coverage at the apex of adspecies A increases with the diffusion coefficient (see Figs. 4a and 4b). The opposite situation occurs at the flanks (see Figs. 4c and 4d). As the diffusion coefficient $D_{\rm A}$ increases, we observe in Fig. 4 that the curves converge towards the result predicted by the multiscale analysis for the infinite-diffusion limit, which confirms in this case the validity of Eqs. (59)-(60).

2. Model II: The unreactive system in the presence of electric field

Let us now consider the case when an electric field is applied, as provided by Model II in Table I. In this case, both the adsorption and desorption rates in Eq. (8) are space dependent. Accordingly, the potential provided by Eq. (30)

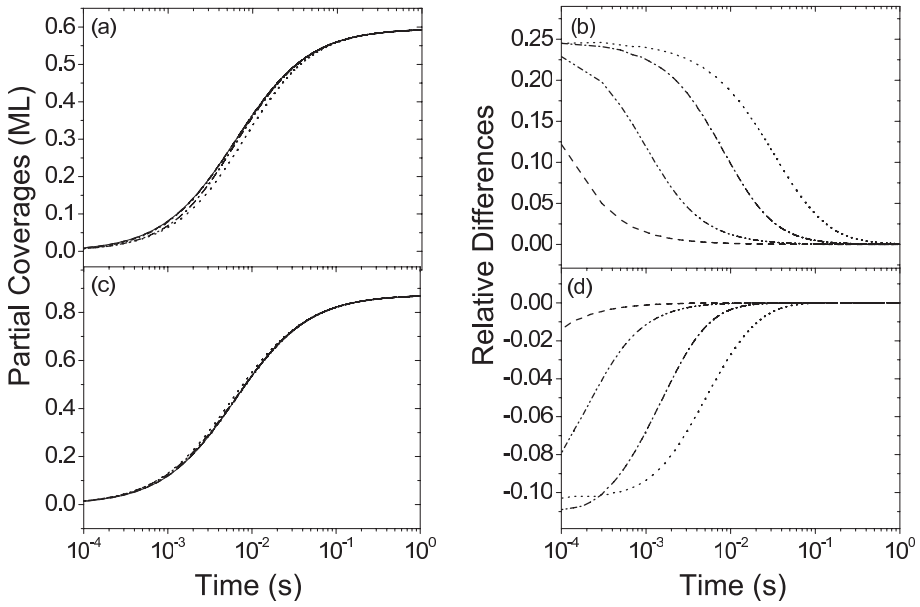

FIG. 4: The partial coverage build-up curves for adspecies A at ring (a) $i = 20$ and (c) $i = 75$ for the dimeric case ($m = 2$) in the absence of both the A+B reaction and an electric field, with an inhomogeneous distribution for adspecies B as in Fig. 3. Curves obtained for $D_{\rm A}/R^2 = 10^{\gamma}$ s^{-1}, with $\gamma = 1$ (dot), $\gamma = 2$ (dash-dot), $\gamma = 3$ (dash-dot-dot), $\gamma = 4$ (dash), and for the quasi-equilibrium distribution ($D_{\rm A} = \infty$) (continuous line). Associated to plots (a) and (c), the evolution of the relative differences of partial coverage with respect to the quasi-equilibrium distribution $[\theta_{\rm A}(D_{\rm A} = \infty) - \theta_{\rm A}(D_{\rm A})]/\theta_{\rm A}(D_{\rm A} = \infty)$: at (b) ring $i = 20$ and at (d) ring $i = 75$. Here, we have considered $\mu_{\rm A}(t = 0) = -1.4$ eV and the other parameters as in Figs. 2 and 3 (see Model I in Table I).

will differ from one ring to another and non-vanishing diffusion currents, as given by Eq. (44), will arise.

We first consider the monomeric case ($m = 1$) in the presence of an electric field. Since the adsorption and desorption rates are now space dependent, the dynamics of adspecies A varies with the value of the diffusion coefficient $D_{\rm A}$, as shown in Fig. 5. This is in contrast to the behavior seen in Fig. 3 for zero electric field. In Fig. 5, we already observe the convergence of the curves for increasing values of the diffusion coefficient $D_{\rm A}$ towards the quasi-equilibrium solution given by Eqs. (59)-(60). This convergence is examined in more detail in Fig. 6. As can be seen in Fig. 6a, the curve for $D_{\rm A}/R^2 = 10^6$ s^{-1} is already very close to the quasi-equilibrium solution over nearly the whole time interval considered. Figure 6b depicts the relative difference with respect the quasi-equilibrium curve, showing its progressive vanishing as the diffusion coefficient increases up to the value $D_{\rm A}/R^2 = 10^6$ s^{-1}. The difference of the potential (30) between a ring at the flanks of the tip and one near the apex of the tip is shown in Fig. 6c. This difference in the potential is expected to vanish in the quasi-equilibrium limit, which is well confirmed by the numerical simulation.

The exactitude of the quasi-equilibrium solution will depend on the value of w used in Eq. (59). As shown in Fig. 7, using the value $w = 1$ instead of Eq. (60) in Eq. (59) can be regarded as an excellent approximation to the infinite-diffusion limit. This approximation was used in the study of a kinetic model of catalytic reactions observed with field ion microscopy [10–12]. However, the choice of the weight $w = 1$ is only an approximation, which can be improved by using the weight (60) obtained by multiscale analysis.

Figure 8 depicts the coverage uptake curves in the dimeric case ($m = 2$) in the presence of an electric field. Here also, the convergence towards the quasi-equilibrium solution is confirmed.

An important role is played by the external electric field on diffusion. This role can be evidenced by considering the diffusion rate defined as

$$\mathcal{D}_{\rm A} \equiv -\boldsymbol{\nabla} \cdot \mathbf{J}_{\rm A} \,. \tag{76}$$

For a zero electric field, the local energy potential is uniform, $\boldsymbol{\nabla}\varepsilon_{\rm A} = 0$, so that the last term of Eq. (21) vanishes in the diffusive current. In this case, the diffusive current is driven by either transient non-uniformities in the coverage of adspecies A or by stationary non-uniformities in the coverage of adspecies B, as shown by Eq. (21). In the presence of an electric field, non-uniformities are also generated by the local energy potential, which may deeply influence the diffusion processes at the field strengths of about $F \simeq 10$ V/nm used in field emission microscopy.

Already in the monomeric case depicted in Fig. 5, we observe the effects introduced by the non-uniformity of the

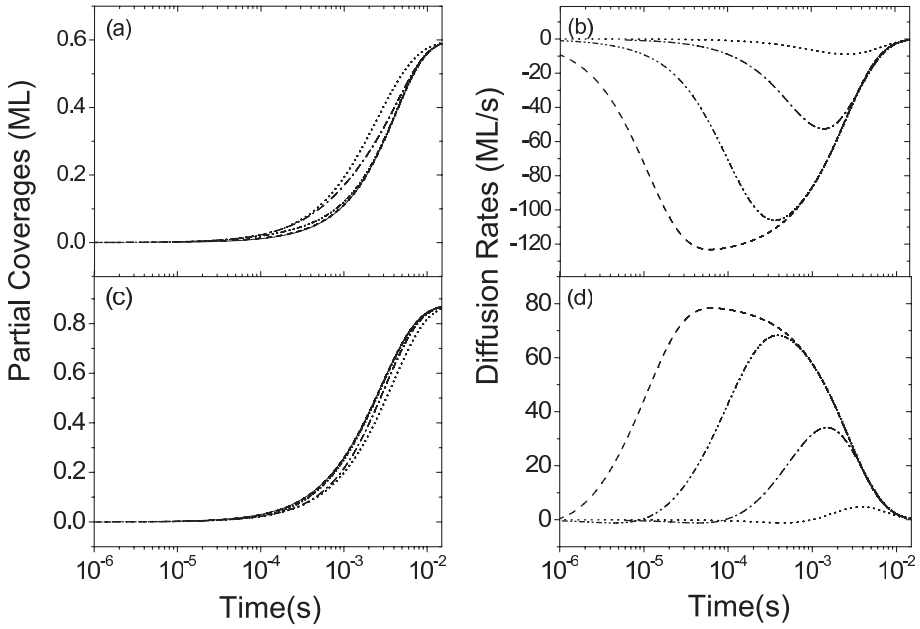

FIG. 5: For the same system as in Fig. 3 (monomeric case), in the presence of an electric field: at ring $i = 20$ (a) the partial coverages and (b) the diffusion rates; at ring $i = 75$ (c) the partial coverages and (d) the diffusion rates. Curves obtained for $D_{\rm A}/R^2 = 10^{\gamma}$ s^{-1}, with $\gamma = 1$ (dot), $\gamma = 2$ (dash-dot), $\gamma = 3$ (dash-dot-dot), $\gamma = 4$ (dash), and for the quasi-equilibrium distribution ($D_{\rm A} = \infty$) (continuous line). The electric field applied was $F = 10$ V/nm, while $d_{\rm d}^{\rm A} = 0.02$ eV nm V^{-1} and $\alpha_{\rm A} = 1 \times 10^{-3}$ eV nm^2 V^{-2} (Model II of Table I).

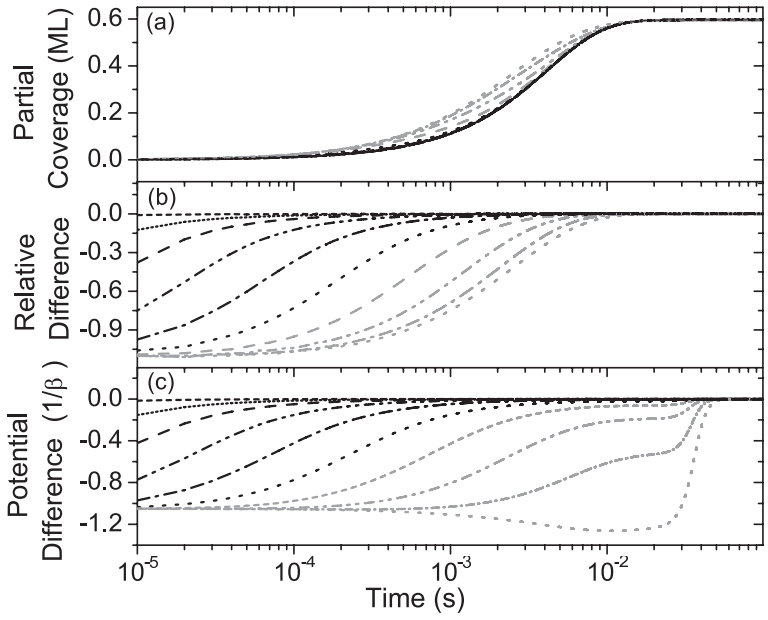

FIG. 6: Convergence towards the infinite-diffusion limiting case for the same system as in Fig. 5 (monomeric case): (a) the partial coverages at ring $i = 20$, (b) the relative differences of coverage evolution with respect to the quasi-equilibrium distribution, (c) the difference of the generalized chemical potential (30) between the rings $i = 20$ and $i = 75$. Curves for different values of $D_{\rm A}/R^2 = 10^{\gamma}$ s^{-1}, as follows: $\gamma = 1$ (grey dot), $\gamma = 1.5$ (grey dot-dash), $\gamma = 2$ (grey dash-dot-dot), $\gamma = 2.5$ (grey dash), $\gamma = 3$ (black dot), $\gamma = 3.5$ (black dash-dot), $\gamma = 4$ (black dash-dot-dot), $\gamma = 4.5$ (black dash), $\gamma = 5$ (black short dot), $\gamma = 6$ (black short dash), and for the quasi-equilibrium distribution ($D_{\rm A} = \infty$) (continuous line) (Model II in Table I).

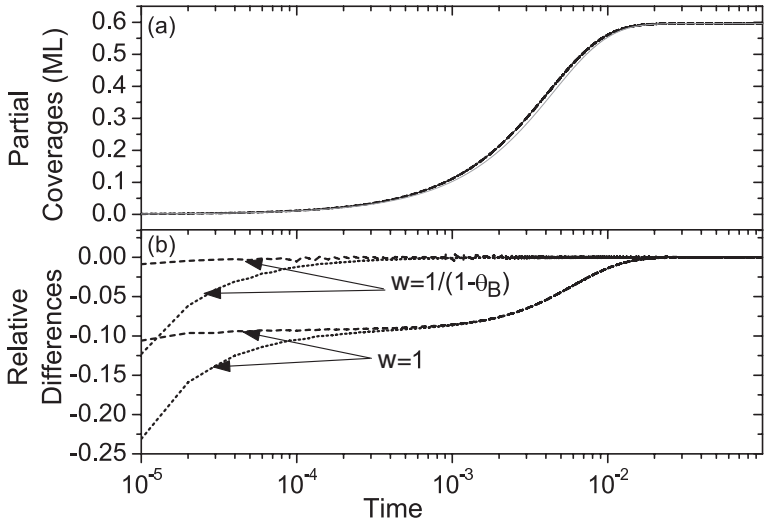

FIG. 7: For the same system as in Figs. 5 and 6 (monomeric case), comparison for the quasi-equilibrium solution using two different values of w in Eq. (59) as indicated in the figure: (a) the partial coverages at ring $i = 20$ and (b) the relative difference of partial coverages with respect to the quasi-equilibrium distribution using the two different values of w. The continuous grey line in the upper panel is the quasi-equilibrium solution with $w = 1$ while the other line types have the same meaning as in Fig. 6 for the value of $D_{\rm A}/R^2$ that was used (Model II of Table I).

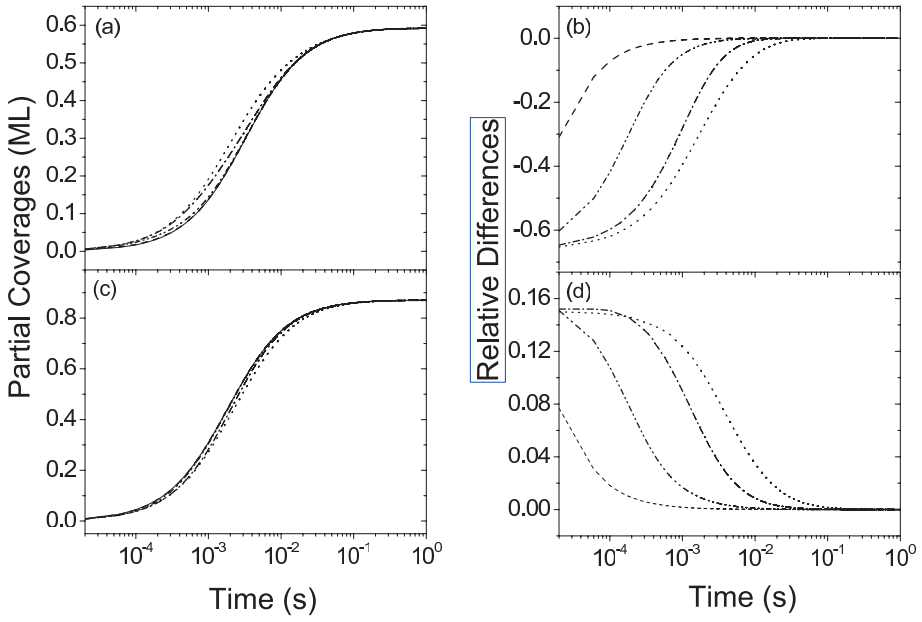

FIG. 8: The partial coverage build-up curves of adspecies A at ring (a) $i = 20$ and (c) $i = 75$ for the same system as in Fig. 4 (dimeric case), but now in the presence of an electric field. The evolution of the relative differences of the partial coverages of adspecies A with respect to the infinite-diffusion case, at rings (b) $i = 20$ and (d) $i = 75$. Curves for different values of $D_{\rm A}/R^2$ as in Fig. 4. Here, we have considered an external electric field of $F = 10$ V/nm, while $d_{\rm d}^{\rm A} = 0.02$ eV nm V^{-1} and $\alpha_{\rm A_2} = 1 \times 10^{-3}$ eV nm^2 V^{-2} (Model II of Table I).

diffusion process when $F \neq 0$. In Fig. 5b, it is shown that the apex is depleted by diffusion since the diffusive rate is thereon negative. The opposite situation occurs at the flanks of the tip where the diffusion rate is positive (see Fig. 5d). This behavior is explained in terms of the gradients of both adspecies. Since the coverage of adspecies B is given by Eq. (71), less sites are available for the active adspecies A at the apex than at the flanks. The first consequence is that the final coverage of adspecies A is lower near the apex than at the flanks (see Figs. 5a and

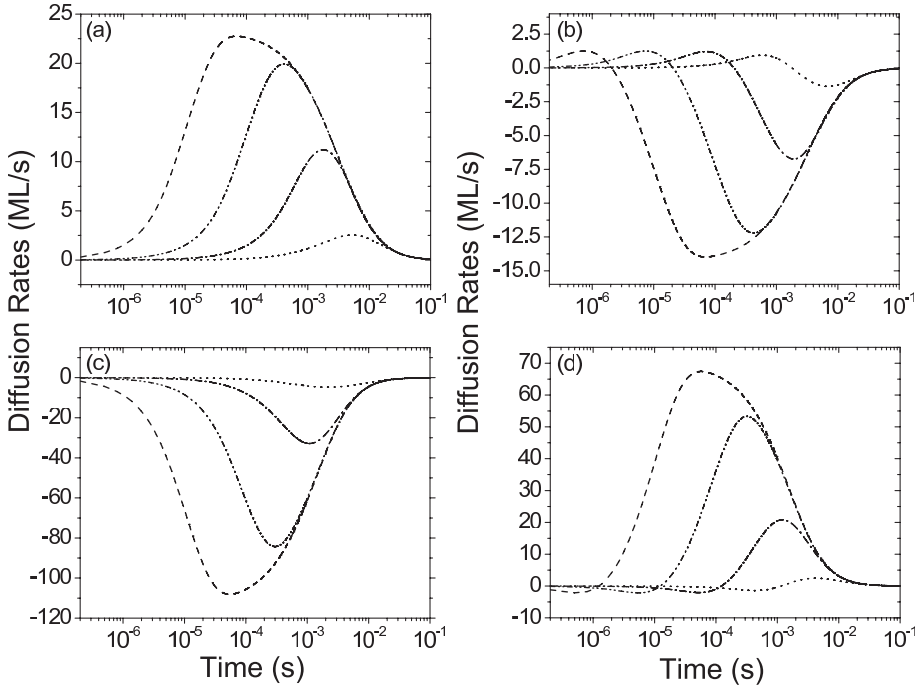

FIG. 9: Evolution of the diffusion rates corresponding to the processes illustrated in Figs. 4 and 8 (dimeric case): in the absence of an electric field, (a) at ring $i = 20$ and (b) at ring $i = 75$; in the presence of an electric field, (c) at ring $i = 20$ and (d) at ring $i = 75$. Curves for different values of $D_{\rm A}$ and $D_{\rm A} = \infty$ as in Figs. 4 and 8 (Model II of Table I).

5c). Moreover, the transient build-up of coverage has opposite trends at the apex and the flanks. As the diffusion coefficient $D_{\rm A}$ increases, the build-up near the apex is delayed while it occurs earlier at the flanks, as observed in Figs. 5a and 5c. Consequently, the coverage of adspecies A tends to be depleted at the apex for larger values of $D_{\rm A}$ while the flanks are further filled.

A similar behavior is observed in Fig. 9 for the dimeric case ($m = 2$), by comparing the diffusion rates in the absence and the presence of an electric field near the apex or at the flanks. As observed in Figs. 9a and 9b for zero electric field, the flanks are depleted by diffusion while the apex is filled. Remarkably, the presence of an electric may completely reverse the situation (see Figs. 9c and 9d). For a non-zero electric field, the apex is now depleted while the flanks are filled, as it was the case in Fig. 5. We observe that the effect of the electric field on diffusion is very important since the electric field has not only reversed the diffusion rate, but also it increased its magnitude by a factor of about five. This is due to the last term in Eq. (21), which is controlled by the gradient of local energy potential:

$$\boldsymbol{\nabla}\varepsilon_{\rm A} = \frac{1}{m}\left(d_{\rm d}^{\rm A} - \alpha_{{\rm A}_m} F\right)\boldsymbol{\nabla} F\,, \tag{77}$$

obtained from Eq. (27) with Eqs. (12) and (11). The first contribution is due to the electric dipolar dependence of the desorption energy barrier and the second to the polarizability of molecules A_m in the gas phase above the surface, which tends to increase the pressure for higher electric fields as described by Eq. (11). Since the electric field is non uniform according to Eq. (67), its gradient is non vanishing and may be the main vector of diffusion for field strengths of the order of 10 V/nm, as demonstrated in Fig. 9.

D. The system in the presence of reaction

In this subsection, we address the effect of considering reactive A and B particles, interacting according to the mechanism described by Eq. (5). Here, we shall assume again the initial distribution of B as given by Eq. (71). Clearly, in order for the effect of the A+B reaction to be observable on the characteristic time scale of the overall process, it has to be shorter than the one of desorption. In particular, we choose the activation energy of process (5) such that $k_{\rm a}^{\rm A} > k_{\rm r} > k_{\rm d}^{\rm A}$. Furthermore, the cases without (Model III in Table I) and with electric field (Model IV) are considered separately.

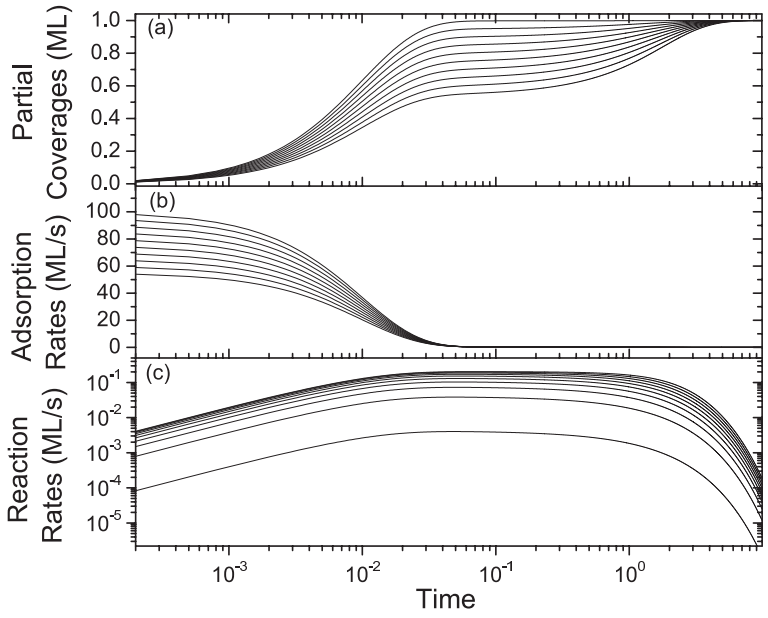

FIG. 10: Monomeric model ($m = 1$) in the presence of an A+B reaction, in absence of an electric field ($F = 0$), and with the same inhomogeneous initial distribution (71) as in Fig. 3, for rings $i = 10, 20, ..., 100$: (a) partial coverages (the curve at the bottom of the plot corresponds to the apex and the one at the top to the base of the tip), (b) adsorption rates [as in plot (a), from bottom to top, the adsorption rates of the rings between the apex and the lowest flank] and (c) reaction rates [contrary as in figures (a) and (b), from top to bottom, the rings between the apex and lowest flank]. Here, we consider a reaction energy barrier $E_r = 0.7$ eV and corresponding prefactor $k_r^0 = 1 \times 10^{10}$ s^{-1} (Model III in Table I).

1. *Model III: The reactive system in the absence of electric field*

Figure 10 summarizes the behavior observed in the case of a reaction without a field. Figure 10a depicts the plot of the coverage of different rings. Associated to this, Fig. 10b exhibits the plot of the adsorption rates and Fig. 10c the plot of the corresponding reaction rates. One distinguishes between two stages:

(i) In the case under consideration, the characteristic time scale of the adsorption process is smaller compared to the one of the reaction. Therefore, in a first stage the coverage evolution is determined by the adsorption rate. This is reflected by an initially high adsorption rate and a low reaction rate (see Figs. 10b and 10c). During this first stage, the coverage of adspecies A evolves in similar way to the case without a reaction (see Fig. 3). As the empty sites are filled, the adsorption rate decreases monotonically while the reaction rate gradually increases. Since the initial coverage of adspecies B is 1/2 ML at the apex and zero in the flanks according to Eq. (71), the coverage of adspecies A is lower at the apex than at the flanks as long as the reaction has not yet started (see Fig. 10a). For the same reason, the adsorption rate is higher in the flanks than at the apex (see Fig. 10b). As shown in Figs. 10b and 10c, once most of the empty sites of a ring are filled, the adsorption rate stabilizes to a very low value and the reaction rate attains an intermediate plateau. In our case, it occurs at time $t = 0.05$ s.

(ii) The onset of the above mentioned intermediate plateau corresponds to the beginning of the second stage. The later is now governed by reaction. The empty sites created by the fast desorption of the product AB are progressively occupied by adspecies A. Notice the coexistence of the plateaus at the level of the reaction rate (see Fig. 10c) and the similar ones taking place for the coverage build-up curves (Fig. 10a). The length of such plateaus is determined by the presence of adspecies B in the corresponding rings. The larger the coverage of adspecies B, the more empty sites are created by the reaction and thus the larger the intermediate plateau will be. Finally, all the adspecies B are depleted by the reaction and the coverage of adspecies A saturates at its maximum possible value $\theta_A \simeq 1$ ML on all the rings.

Concerning the effect of diffusion, similarly as in the case without reaction (Fig. 2), the coverage build-up curves are independent of the diffusion rates in the absence of an electric field.

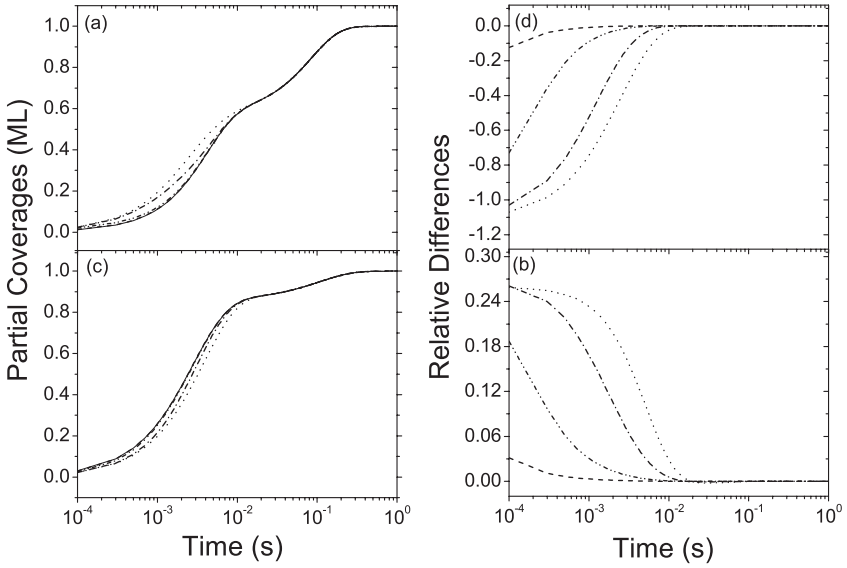

FIG. 11: Monomeric case ($m = 1$) in presence of both an A+B reaction and an electric field, with the same inhomogeneous initial distribution (71) as in Fig. 3: partial coverages at ring (a) $i = 20$ and ring $i = 75$; relative differences of the partial coverages with respect to the infinite diffusion limiting case at (b) ring $i = 20$ and (d) ring $i = 75$. Curves for different values $D_{\rm A}$ and $D_{\rm A} = \infty$ as in Figs. 4 and 8. The parameter values used are $F = 10$ V/nm, $d_{\rm d}^{\rm A} = 0.02$ eV nm V^{-1}, $\alpha_{\rm A} = 1 \times 10^{-3}$ eV nm^2 V^{-2}, and $d_{\rm r} = 0.01$ eV nm V^{-1} (Model IV of Table I).

2. Model IV: The reactive system in the presence of electric field

Let us now consider the influence of an external electric field. With this aim, we use the parameters in Model IV of Table I. The external electric field introduces here an inhomogeneity at the level of the adsorption rate as it was the case in the absence of a reaction. Consequently, a non-vanishing diffusion current arises across the different rings and the coverage evolution becomes dependent on the value of $D_{\rm A}$. As shown in Fig. 11, such a dependence is however limited to the adsorption-dominated stage. Actually, since $k_{\rm a}^{\rm A} > k_{\rm r}$, the coverage dynamics along the first stage is very similar to the one observed in Model II (Fig. 9): at the apex (Figs. 11a and 11b) the coverage rate decreases when increasing $D_{\rm A}$ and the opposite situation occurs at the flank of the tip (Figs. 11c and 11d).

At the end of the adsorption stage, the tip has been partially covered with adspecies according to the quasi-equilibrium distribution given by Eq. (39). Afterwards, the system continues to evolve under quasi-equilibrium conditions, as governed by the dynamics of the chemical potential, which is mainly determined by the reaction of adspecies A and B to the product species AB. This explains why the diffusion rates vanish after the first adsorption stage. On the other hand, comparing the plots of Figs. 10a, 11a, and 11c, one finds that the duration of the first stage is shorter compared to the one without field. The beginning of the second stage now occurs at $t = 0.01$ s, while in absence of the electric field it does at about $t = 0.05$ s. Such a shortening effect is a consequence of the enhanced adsorption rate induced by the electric field. This situation is well illustrated by the plot of the dynamics of the adsorption rate at the apex (Fig. 12). Notice that the adsorption rate attains a much higher value as compared to the case without a field (Fig. 10b).

On the other hand, Fig. 12 shows that the adsorption rate decreases faster with lower values of $D_{\rm A}$. The latter is a consequence of the fact that, at the apex, the number of available sites is depleted faster for low $D_{\rm A}$ values. Indeed, the coverage for adspecies A increases to higher values when one decreases the diffusion coefficient's value (Fig. 11a).

Another interesting field-induced effect is the influence of the field-dipole interaction on the reaction process introduced in Eq. (5). In fact, in the present system a positive (negative) dipole-field interaction reduces the activation barrier for the formation of the product species AB, resulting in a larger (smaller) turnover frequency. If the later is enhanced, the corresponding intermediate plateau region in the coverage build-up curve is reduced. The opposite effect occurs when the reaction is hindered. Figure 13a shows a similar plot as in Fig. 11, now with a larger positive

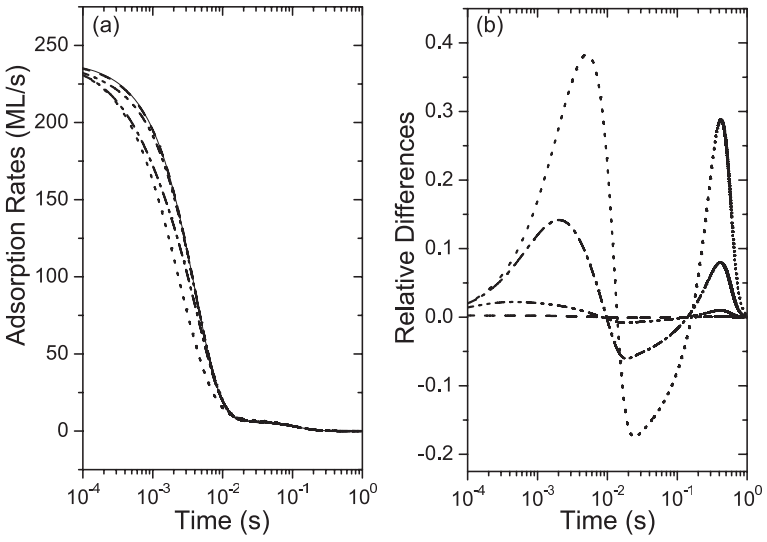

FIG. 12: (a) Evolution of the adsorption rate corresponding to the coverage process depicted in Fig. 11a (ring $i = 20$). (b) Relative differences of the adsorption rate relative to the infinite diffusion limiting case. Curves for different values of $D_{\rm A}$ as in Fig. 4.

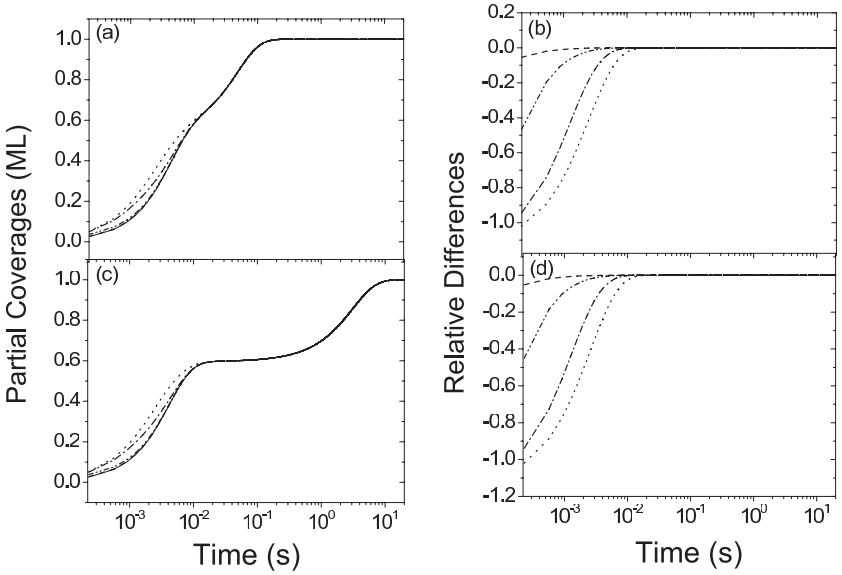

FIG. 13: For the same system as in Fig. 11, the partial coverage at ring $i = 20$. Now with dipole values (a) $d_{\rm r} = 0.012$ eV nm V^{-1} and (b) $d_{\rm r} = -0.002$ eV nm V^{-1}. Curves for different values of $D_{\rm A}$ as in Fig. 4.

value for the dipole. The case of a negative dipole is exhibited in the plot of Fig. 13b. Comparing these figures with Fig. 11a, one notices that the intermediate plateau is shortened in the case of a larger positive dipole (a lower energy barrier), while it is stretched in the case of a negative dipole (a higher energy barrier).

VI. CONCLUSIONS

In this paper, we have carried out a study of ultrafast diffusion in a highly heterogeneous medium as encountered in catalysis and field emission microscopy. As a vehicle of our study, we have considered ultrafast diffusion within an approach based on macroscopic reaction-diffusion equations describing the processes of adsorption, desorption, and reaction of two adspecies on a paraboloidal heterogeneous surface in the presence of an external electric field. An

expression for the time evolution of this system was derived in the ultrafast-diffusion limit using a multiscale analysis. If the diffusion of one of the adspecies is much faster than the other processes taking place in the system, this adspecies rapidly reaches a quasi-equilibrium spatial distribution, which thereafter slowly evolves in time in a way controlled by a single time-dependent parameter, which is a nonequilibrium chemical potential of the fast adspecies. Thanks to our multiscale analysis, we obtain an equation for the time evolution of this nonequilibrium chemical potential in terms of the rates of the slow processes. Its time evolution is globally determined by averaging the local rates with the specific weight (60), which is the central result of this paper. This weight depends on the coverage of the slow adspecies and is thus spatially dependent if the later is.

The validity of this result is confirmed by numerical simulations under different conditions in the absence or presence of an electric field or a reaction. In these simulations, the time evolution of the reaction-diffusion equations for increasing values of the diffusion coefficient has been compared with the result of the infinite-diffusion limit. The numerical results confirm the convergence towards the predictions of Eqs. (59)-(60) obtained by a multiscale analysis. The advantage of these equations is that the partial differential reaction-diffusion equation (PDE) is replaced by an ordinary differential equation (ODE) for the nonequilibrium chemical potential of the quasi-equilibrium distribution in the case of ultrafast diffusion. The numerical integration of the ODE is much faster and easier to implement than the one of the PDE.

We have also considered the approximation where the weight is uniform. This approximation turns out to give results in good agreement with those based on the exact weight (60), which justifies the choice of this approximation as used in our previous modeling [10–12].

Moreover, our results clearly show that electric fields of the order of 10 V/nm may influence so much the diffusion of adspecies that the diffusion rate is dominated by their effect. Such field-induced effects have their origin in the fact that the diffusive current of an adspecies includes a term that depends on the gradient of the local energy potential acting on the particles, as described by Eq. (21). For field strengths encountered at the nanometric tip of a field emission microscope, this term dominates the diffusive current, which may significantly enhance or even reverse the diffusion rates as compared to situations in the absence of an electric field.

The multiscale analysis carried out in the present paper is general and applies to many possible systems beyond the cylindrically symmetric systems investigated in our numerical simulations. The results (59)-(60) of the multiscale analysis also apply to ultrafast diffusion on field emitter tips which are anisotropic due to the underlying crystalline structure [10–12]. In such systems, the adsorption, desorption, and reaction rates have a local spatial dependence on the orientation of the local crystal plane at every point of the surface. In spite of this complication, the quasi-equilibrium approach we have here developed continues to apply and the time evolution is ruled by Eqs. (59)-(60) in the ultrafast diffusion limit.

Acknowledgments

JSM acknowledges support from the F.R.S.-FNRS Belgium. This research is financially supported by the "Communauté française de Belgique" (project "Actions de Recherche Concertées" No. 04/09-312) and by the Belgian Federal Government (project IAP "NOSY").

APPENDIX A: SPATIAL DISCRETIZATION

The paraboloid of Fig. 1 is partitioned into N rings:

$$i = 0: \qquad 0 \le \eta < \frac{1}{2}\Delta\eta\,, \tag{A1}$$

$$i = 1, 2, ..., N-1: \qquad \eta_{i-\frac{1}{2}} \le \eta < \eta_{i+\frac{1}{2}}\,, \tag{A2}$$

having the boundaries

$$\eta_{i\pm\frac{1}{2}} = \eta_i \pm \frac{1}{2}\Delta\eta\,. \tag{A3}$$

The partial coverages $\theta_{\mathrm{A}i} \equiv \theta_i$ and $\theta_{\mathrm{B}i}$ as well as the other space-dependent quantities are evaluated in the middle of the rings at $\eta_i = i\Delta\eta$ $(i = 0, 1, 2, ..., N-1)$. According to Eq. (69), the surface area of the ring i is given by

$$A_i = \pi R \sqrt{1 + \frac{\eta_i}{R}}\,\Delta\eta\,. \tag{A4}$$

We introduce the current or flux across the boundary between the rings i and $i+1$ as

$$I_{i,i+1} \equiv \int \mathbf{J} \cdot d\mathbf{S}\,, \tag{A5}$$

where $\mathbf{J} \equiv \mathbf{J}_{\rm A}$ is the current density of the ultrafast adspecies A at $\eta_{i+\frac{1}{2}}$ and $d\mathbf{S} = \mathbf{n}\rho_{i+\frac{1}{2}}d\varphi$ is the element of the circular boundary of radius $\rho_{i+\frac{1}{2}} = \sqrt{R\,\eta_{i+\frac{1}{2}}}$ in the direction of the unit vector $\mathbf{n}$ normal to the boundary of the ring but parallel to the surface. The balance equation for the number $\mathcal{N}_i = A_i\theta_i$ of particles of adspecies A in the ring i is thus given by

$$A_i\frac{d\theta_i}{dt} = A_i\mathcal{S}_i - \frac{1}{\epsilon}(I_{i,i+1} - I_{i-1,i}) \qquad (i = 0, 1, 2, ..., N-1)\,, \tag{A6}$$

where $\mathcal{S}_i = \mathcal{S}_{\rm A}(\theta_{{\rm A}i}, \theta_{{\rm B}i})$ with $\mathcal{S}_{\rm A} = \mathcal{R}_{\rm A}$ and ϵ is the same fictitious parameter as introduced in Eq. (40) to take into account the ultrafast diffusion of adspecies A in the limit $\epsilon \to 0$. Moreover, we impose reflection boundary conditions at the apex and at $\eta = (N-1)\Delta\eta$ so that $I_{-1,0} = I_{N-1,N} = 0$.

Here, we assume that diffusion is isotropic so that the tensor of linear-response coefficients in Eq. (29) is the scalar quantity

$$L = L_{\rm A} = D_{\rm A}\,\theta_{\rm A}\,(1 - \theta_{\rm A} - \theta_{\rm B})\,. \tag{A7}$$

Accordingly, the current density is proportional to the gradient of the potential $\Phi = \Phi_{\rm A}$ given by Eq. (30):

$$\mathbf{J} = -L\,\boldsymbol{\nabla}\Phi\,. \tag{A8}$$

Both quantities L and Φ are evaluated in the middle of each ring at η_i. Now, the flux (A5) between the rings i and $i+1$ can be approximated by the expression

$$I_{i,i+1} = -\frac{L_i + L_{i+1}}{2}\,\frac{\Phi_{i+1} - \Phi_i}{\Delta_{i+\frac{1}{2}}}P_{i+\frac{1}{2}}\,, \tag{A9}$$

where

$$\Delta_{i+\frac{1}{2}} = \sqrt{1 + \frac{R}{\eta_{i+\frac{1}{2}}}}\,\frac{\Delta\eta}{2}\,, \tag{A10}$$

is the distance between the middles of the rings i and $i+1$ given by Eq. (65) and

$$P_{i+\frac{1}{2}} = 2\pi\rho_{i+\frac{1}{2}} = 2\pi\sqrt{R\,\eta_{i+\frac{1}{2}}}\,, \tag{A11}$$

is the perimeter of the boundary between these rings.

The multiscale analysis is carried out for the discretized reaction-diffusion equations as in the continuous case by first expanding the partial coverage of the ultrafast adspecies A in powers of the small parameter:

$$\theta_i = \theta_i^{(0)} + \epsilon\,\theta_i^{(1)} + O(\epsilon^2)\,. \tag{A12}$$

At the leading order, we obtain the conditions

$$\Phi\left(\theta_i^{(0)}\right) = \Phi\left(\theta_{i+1}^{(0)}\right)\,, \tag{A13}$$

which are equivalent to the vanishing of the fluxes, $I_{i,i+1}^{(0)} = 0$, and which leads to the quasi-equilibrium distribution

$$\theta_i^{(0)} = \theta_{{\rm A}i}^{(0)} = \frac{1 - \theta_{{\rm B}i}}{1 + \zeta\left(\frac{k_{{\rm d}i}^{\rm A}}{k_{{\rm a}i}^{\rm A}P_{{\rm A}i}}\right)^{\frac{1}{m}}}\,, \tag{A14}$$

where the quantity

$$\zeta = {\rm e}^{-\beta\left[\mu_{\rm A}(t) - \mu_{\rm A}^{\rm eq}\right]} \tag{A15}$$

depends on time but not on space and takes the value $\zeta = 1$ at equilibrium. We notice that Eq. (A14) is the discrete version of the quasi-equilibrium distribution (39).

At the next-to-leading order, we obtain a set of coupled equations forming the following system of inhomogeneous linear equations:

$$\hat{\mathcal{L}}|\theta_i^{(1)}\rangle = |q_i^{(0)}\rangle \tag{A16}$$

with the discretized version of the linear operator (53) and

$$q_i^{(0)} = \frac{d\theta_i^{(0)}}{dt} - \mathcal{S}(\theta_i^{(0)})\,. \tag{A17}$$

According to the theorem of Fredholm alternative [13], this system can be solved if the right-hand side is orthogonal to the null eigenvector of the adjoint operator

$$\hat{\mathcal{L}}^\dagger|g_i\rangle = 0\,. \tag{A18}$$

The null eigenvector is given by

$$g_i = b\,A_i\,, \tag{A19}$$

with constant b. Consequently, the solvability condition $\langle g_i|q_i^{(0)}\rangle = 0$ reads

$$\sum_i A_i \left[\frac{d\theta_i^{(0)}}{dt} - \mathcal{S}(\theta_i^{(0)})\right] = 0\,. \tag{A20}$$

Substituting the expression (A14) for the quasi-equilibrium coverage $\theta_i^{(0)} = \theta_{\mathrm{A}i}^{(0)}$, we finally obtain the following ordinary differential equation for the nonequilibrium chemical potential of adspecies A:

$$\frac{d\mu_{\mathrm{A}}}{dt} = \frac{\sum_i w_i \left[(1-\theta_{\mathrm{B}i})\,\mathcal{S}_{\mathrm{A}}(\theta_{\mathrm{A}i}^{(0)},\theta_{\mathrm{B}i}) + \theta_{\mathrm{A}i}^{(0)}\,\mathcal{S}_{\mathrm{B}}(\theta_{\mathrm{A}i}^{(0)},\theta_{\mathrm{B}i})\right]}{\beta\,\sum_i w_i\,\theta_{\mathrm{A}i}^{(0)}\,(1-\theta_{\mathrm{A}i}^{(0)}-\theta_{\mathrm{B}i})}\,, \tag{A21}$$

with the weights

$$w_i = \frac{A_i}{1-\theta_{\mathrm{B}i}} \tag{A22}$$

in the rings $i = 0, 1, 2, ..., N-1$. This result is clearly the discrete version of Eqs. (59) and (60), which confirms the multiscale analysis in the continuous case and allows its numerical implementation.

---

[1] G. Nicolis and I. Prigogine, *Self-Organization in Nonequilibrium Systems* (Wiley, New York, 1977).
[2] P. Gaspard and G. Nicolis, J. Stat. Phys. **31**, 499 (1983).
[3] S. K. Scott, *Chemical Chaos* (Clarendon Press, Oxford, 1991).
[4] M. T. M. Koper, P. Gaspard, and J. H. Sluyters, J. Chem. Phys. **97**, 8250 (1992).
[5] A. Goldbeter, *Biochemical Oscillations and Cellular Rhythms* (Cambridge University Press, Cambridge UK, 1996).
[6] I. R. Epstein and J. A. Pojman, *An Introduction to Nonlinear Chemical Dynamics* (Oxford University Press, New York, 1998).
[7] J. Ross, I. Schreiber, and M. O. Vlad, *Determination of Complex Reaction Mechanisms: Analysis of Chemical, Biological, and Genetic Networks* (Oxford University Press, New York, 2005).
[8] T. Erneux and A. Goldbeter, SIAM J. Appl. Math. **67**, 305 (2006).
[9] T. Erneux, *Applied Delay Differential Equations* (Springer, New York, 2009).
[10] J.-S. McEwen, P. Gaspard, T. Visart de Bocarmé, and N. Kruse, Proc. Natl. Acad. Sci. USA **106**, 3006 (2009).
[11] J.-S. McEwen, P. Gaspard, T. Visart de Bocarmé, and N. Kruse, J. Phys. Chem. C **113**, 17045 (2009).
[12] J.-S. McEwen, P. Gaspard, T. Visart de Bocarmé, and N. Kruse, Surf. Sci. **604**, 1353 (2010).
[13] G. Nicolis, *Introduction to Nonlinear Science* (Cambridge University Press, Cambridge UK, 1995).
[14] E. A. Guggenheim, *Encyclopedia of Physics, Vol. III/2* (Springer-Verlag, Berlin, 1959), pp. 1–118.
[15] S. R. de Groot and P. Mazur, *Non-Equilibrium Thermodynamics* (Dover, New York, 1984).

[16] R. Gomer, Rep. Prog. Phys. **53**, 917 (1990).
[17] A. S. Mikhailov and G. Ertl, Chem. Phys. Lett. **238**, 104 (1995).
[18] G. Giacomin and J. L. Lebowitz, Phys. Rev. Lett. **76**, 1094 (1996).
[19] Y. De Decker, H. Marbach, M. Hinz, S. Günther, M. Kiskinova, A. S. Mikhailov, and R. Imbihl, Phys. Rev. Lett. **92**, 198305 (2004).
[20] M. K. Miller, A. Cerezo, M. G. Hetherington, and G. D. W. Smith, *Atom Probe Field Ion Microscopy*, Monographs on the Physics and Chemistry of Materials (Clarendon, Oxford, 1996).
[21] L. Pauling and E. B. Wilson Jr., *Introduction to Quantum Mechanics with Applications to Chemistry* (Dover, New York, 1985).